Dimeric and Trimeric Uranyl(VI)–Citrate Complexes in Aqueous Solution

Kretzschmar, J.; Tsushima, S.; Lucks, C.; Jäckel, E.; Meyer, R.; Steudtner, R.; Müller, K.; Roßberg, A.; Schmeide, K.; Brendler, V.;

Originally published:

May 2021

Inorganic Chemistry 60(2021)11, 7998-8010

DOI: https://doi.org/10.1021/acs.inorgchem.1c00522

On the dimeric and trimeric uranyl(VI)–citrate complexes in aqueous solution

Jerome Kretzschmar,[†] Satoru Tsushima,[†‡] Christian Lucks,[†§#] Elisabeth Jäckel,[†] Ronny Meyer,[†] Robin Steudtner,[†] Katharina Müller,[†] André Rossberg,[†§] Katja Schmeide,[†] and Vinzenz Brendler[†]*

† Helmholtz-Zentrum Dresden-Rossendorf e.V., Institute of Resource Ecology, Bautzner Landstr. 400, 01328 Dresden, Germany.

‡ World Research Hub Initiative (WRHI), Institute of Innovative Research, Tokyo Institute of Technology, Meguro, 152–8550 Tokyo, Japan.

§ Rossendorf Beamline (ROBL, BM20-CRG), European Synchrotron Radiation Facility, 6 rue Jules Horowitz, BP 220, 38043 Grenoble, France

ABSTRACT

This research addresses a subject discussed controversially for almost 70 years. The interactions between the uranyl(VI) ion, U(VI), and citric acid, H_3Cit, were examined by a multi-method approach comprising NMR, UV-Vis, ATR FT-IR, and EXAFS spectroscopies as well as DFT calculations. Combining ^{17}O NMR and DFT calculation allowed an unambiguous decision on complex configurations, evidencing for the first time that the dimeric complex, $(UO_2)_2(HCit_{-H})_2^{2-}$, exists as two diastereomers, with the *syn* isomer in aqueous solution strongly favored over the *anti* isomer. Both isomers interconvert mutually, with exchange rates of ~30 s^{-1} at −6 °C and ~249 s^{-1} at 60 °C in acidic solution, corresponding to an activation barrier of about 24 kJ mol^{-1}. Upon increasing pH, ternary dimeric mono- and bis-hydroxo as well as trimeric complexes form, *i.e.* $(UO_2)_2(HCit_{-H})_2(OH)^{3-}$, $(UO_2)_2(HCit_{-H})_2(OH)_2^{4-}$, $(UO_2)_3(O)(Cit_{-H})_3^{8-}$, and $(UO_2)_3(O)(OH)(Cit_{-H})_2^{5-}$, respectively. Stability constants were determined for all dimeric and trimeric species, with

log $\beta°$ = −(8.6 ± 0.2) for the 3:3 species being unprecedented. Additionally, in the 6:6 sandwich complex, formed from two units 3:3 species, the ^{17}O NMR resonance of the trinuclear uranyl(VI) core bridging μ_3-O is shown for the first time. Species distribution calculations suggest that the characterized polynuclear uranium(VI)-citate species do not significantly increase uranium(VI) mobility in the environment. Furthermore, we revise the misconceptions in aqueous U(VI)-citric acid solution chemistry, *i.e.* structures proposed and repeatedly taken up, and outline generalized isostructural considerations to provide a basis for future uranium(VI) complexation studies.

INTRODUCTION

Chemical background

Sources for uranium, U, in the biogeosphere are manifold. Weathering of soils and rocks can release it into ground water. Diverse technological processes can enhance and also release naturally occurring U in the environment; for instance, ore mining and processing, drinking and waste water treatment, oil and gas production, or geothermal engineering.

As one of the most important sources for electrical power supply, U is key component in nuclear fuel[4, 5] and, consequently, major part of both the uranium processing cycle and nuclear waste.[6] Adequate treatment of nuclear waste as well as operation and remediation of U legacies and contaminations due to nuclear incidents require comprehensive examination of its interaction with biotic and abiotic components.

Under aqueous aerobic conditions, U prevails in hexavalent state, U(VI), forming readily water-soluble, mobile, and bioavailable species. Characteristic for high-charged ions of actinides in +V and +VI valence state it bears two ‘actinyl’ oxygen atoms (O_{yl}) linearly bound by multiple bonds, in case of U yielding the highly stable uranyl(VI) ion, UO_2^{2+}. The effective charge of about 3.3 determines the strength of its complexes. As ligand coordination is limited to the 'equatorial' plane, *i.e*. perpendicular to the O_{yl}–U–O_{yl} axis, complex stoichiometries are influenced by the ligand's denticity and/or steric demands.

Citric acid is a hydroxy-tricarboxylic acid. Being a ubiquitous molecule and an essential and highly concentrated constituent in aerobic organisms, it is eponymous for the citric acid cycle as their key metabolic pathway. *In vivo*, actinides are commonly bound to a protein-fraction such as transferrins as well as to a fraction of small anionic complexing agents.[7] The latter are primarily constituents of the citric acid cycle easily complexing HSAB-hard cations such as UO_2^{2+}.[8, 9] Incorporated actinides are mainly excreted with the urine, primarily citrate-bound.[10-15]

Citric acid, CA, has four functional groups, *i.e.* one hydroxyl group and three carboxyl groups (Figure 1A), all of which are potential binding sites. Accordingly, CA easily chelates metal ions in very stable complexes. In aqueous solution the hydroxyl group is a notably weak acid. However, upon coordination to strong Lewis acids its pK_a is drastically lowered so that it deprotonates even under acidic conditions. Moreover, the configuration of CA's binding sites constrains metal ion coordination, so that three functional groups at most can coordinate the same metal ion (*cf.* Figure 1). Thus, while only two COO groups of the same CA ligand can simultaneously bind to one U(VI), the hydroxyl functional group is strongly involved in complexation.[16]

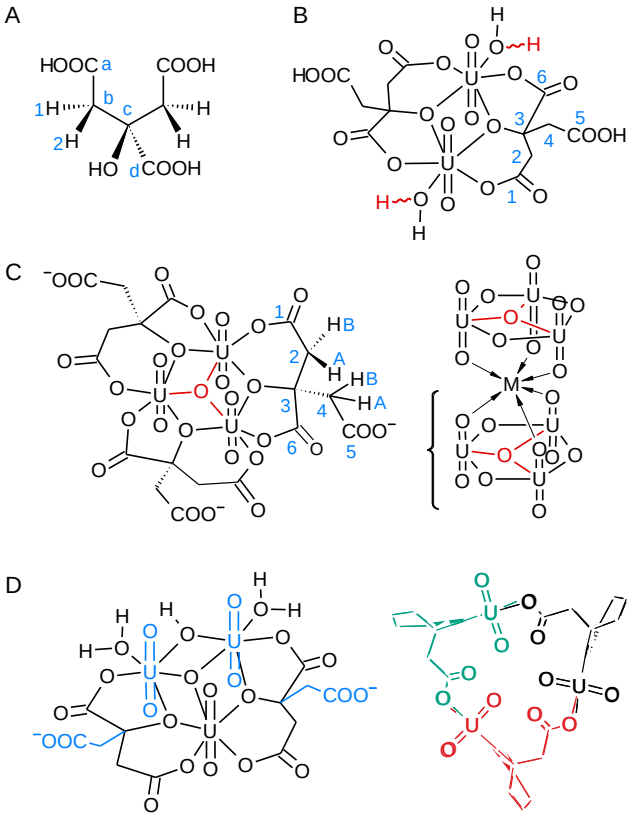

Figure 1. Generic structures of citric acid (A) as well as of aqueous complexes with U(VI):citrate ratio of (B) 2:2, (C) 3:3, and (D) 3:2. For the latter two, the correspondingly formed superstructures are depicted on the right: 6:6 metal ion (M = Na^+, Ca^{2+}, La^{3+}) sandwich complex[17] and 9:6 macrocycle,[18] respectively; for clarity, the structures are reduced to the sites of association.

Considering CA as $H_3Cit_{(aq)}$, successive deprotonation of the carboxyl groups yields H_2Cit^-, $HCit^{2-}$, and Cit^{3-}. The deprotonation of the hydroxyl group, -OH, which is normally not observed in aqueous solutions of free CA but only upon complexation, will be referred to as $HCit_{-H}^{3-}$ or Cit_{-H}^{4-}, respectively.

Complex formation can basically be described according to the following reaction equations:

$$2\ UO_2^{2+} + 2\ Cit^{3-} \rightarrow (UO_2)_2(HCit_{-H})_2^{2-} \equiv 2{:}2, \quad (1)$$

$$2\ UO_2^{2+} + 2\ Cit^{3-} + H_2O \rightarrow H^+ + (UO_2)_2(HCit_{-H})_2(OH)^{3-} \equiv 2{:}2{:}1, \quad (2)$$

$$2\ UO_2^{2+} + 2\ Cit^{3-} + 2\ H_2O \rightarrow 2\ H^+ + (UO_2)_2(HCit_{-H})_2(OH)_2^{4-} \equiv 2{:}2{:}2, \quad (3)$$

$$3\ UO_2^{2+} + 3\ Cit^{3-} + H_2O \rightarrow 5\ H^+ + (UO_2)_3(O)(Cit_{-H})_3^{8-} \equiv 3{:}3, \quad (4)$$

$$3\ UO_2^{2+} + 2\ Cit^{3-} + 2\ H_2O \rightarrow 5\ H^+ + (UO_2)_3(O)(OH)(Cit_{-H})_2^{5-} \equiv 3{:}2, \quad (5)$$

For convenience the complexes are occasionally denoted by their U(VI):CA ratio; in case of the dimeric complexes by their U(VI):CA:OH ratio.

Motivation

Understanding the aqueous chemistry of the uranyl(VI)-CA system is challenging as continuous discussions on complex structures and speciation testify.[16, 18-28] Uranyl(VI) citrate complexes are of great importance regarding uranium's environmental migration as well as for remediation concepts and processes, for instance microbial degradation and immobilization.[29-33] For a sound understanding of the chemical behavior in general and the environmental fate in particular, knowledge of both aqueous speciation and molecular structures in solution is crucial. In addition, verification or falsification of proposed species, and elucidating formation reactions is essential

for correct thermodynamic models and predictive calculations addressing safety and risk assessment for actinide transport in the environment.

Accordingly, this work has the following objectives:

(i) sum up the actual state of knowledge and revise possible misconceptions in aqueous U(VI)-CA solution complex structures proposed and repeatedly taken up;

(ii) examine and discuss dimeric and trimeric complex structures and dynamics, especially the formation and mutual interconversion of isomers due to the chiral centers induced in the ligand upon complexation, as well as reconsider and re-interpret NMR spectroscopic data;

(iii) consolidate thermodynamic data for binary and ternary dimeric species and present novel thermodynamic data on the 3:3 complex; and

(iv) outline generalized isostructural considerations, applicable for future uranium(VI) complexation studies.

State of knowledge

UO_2^{2+} forms complexes with all anionic forms of CA.[16] The (binary) dimeric complex $(UO_2)_2(HCit_{-H})_2^{2-}$ is well established and is by far the most stable ($\log \beta^\circ = 21.3 \pm 0.5$), occurring in a wide pH range, ≈ 2–7.[16] Above pH 4, trimeric species form with U(VI):CA ratios of 3:3 and 3:2, and predominate as of circumneutral conditions up to alkaline solution.[18, 20, 28]

As early as in 1954, it was concluded that CA binds U(VI) by two carboxyl groups and the hydroxy group as a tridentate chelate.[20] Although already stated in early papers that the alcoholic hydroxyl group abstracts its H^+ upon μ_2-bridging between two uranyl units in the dimeric complex ($C3–O<(UO_2)_2$, *cf*. Figure 1B), the erroneous structure drawing this hydrogen bound to the alkoxy oxygen persisted for decades.[22, 24, 26] Allen *et al*.[25] performed X-ray absorption fine-structure (EXAFS) spectroscopy and derived the correct 2:2 complex structure considering Feldman and coworkers' potentiometric and spectrophotometric studies regarding the hydroxyl group. Deprotonation of hydroxyl groups upon metal ion complexation is a very common and likewise challenging question. A protonated μ_2-bridging hydroxyl group ($C–OH<(UO_2)_2$) would constitute a tetravalent oxygen, which is very uncommon by itself and especially in protic solvents, since it would deprotonate instantly as the acidity of this particular proton is drastically increased.

Kakihana *et al*.[23] attempted to bring their infrared (IR) and nuclear magnetic resonance (NMR) spectra into agreement with a 3:2 complex linear structure despite the doubled set of ^{13}C NMR

signals observed (for unspecified sample conditions), presupposing the solution to contain one complex species only. Nunes and Gil[24] performed ^{1}H and ^{13}C NMR spectroscopy. Arguing with the ligands' equivalency a cyclic trimeric 3:2 structure was proposed with two hydroxo groups bridging two uranyl(VI) units, $UO_2(\mu_2\text{-}OH)_2UO_2$. This binuclear moiety is bridged on either uranium by the presumed two ligands to a third uranyl(VI) unit that, for steric constraints, requires an $O_{yl}–U–O_{yl}$ axis perpendicular to those of the binuclear moiety. However, the trimeric species were later shown to contain a trinuclear uranyl(VI) core bridged by an oxide ion (μ_3-O). The same reasoning regarding the ligands' equivalency holds true particularly for the highly symmetric 3:3 complex (*cf*. Figure 1C). The reported features such as one ^{1}H NMR signal being remarkably shifted and the unaltered spectral appearance up to 320 K, and the therefrom drawn conclusion of a rigid structure of unique arrangement in fact pertain to a sandwich superstructure[17] formed by two molecules of the 3:3 species (*vide infra*) instead of the proposed 3:2 complex. Unaware of the coexistence of two trimeric species, additional signals upon increasing pD were ascribed to the deprotonation of the bridging hydroxyl group.

Pasilis and Pemberton[26] performed Raman spectroscopy, ATR FT-IR (attenuated total reflectance Fourier-transform IR) spectroscopy, and ESI-MS (electrospray ionization mass spectrometry), discussing 2:2, 3:3, and 3:2 U(VI)-CA species, denoting the latter two as $(UO_2)_3(Cit)_3^{3-}$ and $(UO_2)_3(Cit)_2^{0}$. The Raman-active band at 826 cm^{-1} was assigned (and later confirmed[18]) to the symmetric uranyl stretching vibration, $\nu_1(UO_2)$, associated with the 2:2 complex. Raman features observed at 812 and 795 cm^{-1} and erroneously ascribed to the 3:2 and 3:3 complex, respectively, were later clarified by Basile *et al*.[18] They also performed Raman spectroscopy, however, of single-crystalline material (800 and 790 cm^{-1}) and in solution upon re-dissolution of the former (797 and 793 cm^{-1}), which allowed for the assignment of $\nu_1(UO_2)$ to the 3:3 and the 3:2 trimeric species, respectively. Especially by their single-crystal X-ray diffraction data the structures of the long proposed 3:3 and 3:2 species (*cf*. Figures 1C and D) were revealed. Moreover, both trimeric species were found to build superstructures in the crystals, *i.e*., two 3:3 species sandwich one sodium ion, and three 3:2 species as stoichiometric sub-units yield a macrocyclic 9:6 complex. Both superstructures were suspected to already form in solution.[18]

Recently, comprehensive NMR studies evidenced the formation of the Na^{+} sandwich complex, corresponding to 6:6 U(VI):CA ratio overall, in pD 7 solution above a concentration of 3 mM each in U(VI) and CA.[17] The sharp ^{1}H and ^{13}C NMR resonances already noticed by Nunes and Gil[24] are

in fact due to the rigid all-*cis* conformation of the unbound -CH_2COO^- moieties due to the sandwich arrangement. Additionally, a corresponding 6:6 U(VI)-CA complex was shown to sandwich Ca^{2+} as well as La^{3+} in aqueous solution.[17]

Berto *et al*.[28] combined potentiometric and spectrophotometric investigations for different background electrolytes and ionic strengths, and reported formation constants and UV-Vis spectra for ternary uranyl(VI) hydroxo citrate dimeric complexes, in general expressed as $(UO_2)_2(Cit)_x(OH)_y$, with either or both x and y being 1 or 2. According to the authors, these ternary species are formed by deprotonation of alcoholic hydroxyl of citrate.

The latter statement reflects both the principal difficulty and limitations of potentiometry in assigning the origin of the detected H^+ since proton abstraction can namely be due to either U(VI) coordination to COOH or C–OH, or simply upon increasing pH to the corresponding pK_a (COOH), or caused by hydrolysis of U(VI)-coordinating water. Therefore, spectroscopic methods should be used at least complementary.

In fact, the polarization of the O–H bonds in H_2O coordinating U(VI) or, in general, any (strong) Lewis acid (M) facilitates abstraction of H^+, *i.e*. decreasing the pK_a of *R*HO→M (*R* = H or organic residue). Related to that, the energetically disfavored abstraction of the alcoholic proton under pH conditions many orders of magnitude below its corresponding pK_a is mainly overcome by strong entropy contributions upon liberating weaker bound coordinating water and enthalpy contribution upon its solvation.

The structures of binary dimeric and of trimeric U(VI)-CA species are well resolved in the crystallized complexes.[18, 34-37] As will be demonstrated, molecular structures can essentially differ between solid state and (aqueous) solution, particularly when dynamic processes take effect. Thus, in order to improve the understanding of the U(VI)-CA system and attaining knowledge on the aqueous solution structures and dynamics, we used a unique multi-method approach, combining NMR, UV-Vis, ATR FT-IR, and EXAFS spectroscopies with DFT calculation.

EXPERIMENTAL SECTION

Materials

General remarks. All preparation steps were performed with safety precautions according to both radio- and chemotoxicity of natural uranium (U-nat). All chemicals were used without further

purification. Covering the samples with aluminum foil protected them from light. NMR samples were prepared with deuterated chemicals (all by Deutero): D_2O, (99.98% D) and D_2O solutions of both NaOD (40% in D_2O with 99% D) and DCl (37% in D_2O with 99% D) for pD adjustment. The latter was according to pD = pH + 0.4, *i.e.*, addition of 0.4 units to the pH meter reading.[38] UO_3 (A = 25.3 kBq g^{-1} U-nat) was dissolved in 0.5 M (denoting mol per liter) $HClO_4$ or DCl with subsequent concentration determination by ICP-MS (Elan 6000, Perkin Elmer), and CA stock solution made from citric acid (Roth, *p.a.*) by weighing required amounts for dissolution in Milli-Q H_2O (18.2 MΩ cm, Millipore) and D_2O, respectively. *NMR samples* comprise seven solutions prepared in D_2O, two of which 250 mM each in U(VI) and CA for both pD 2.5 and 7.5, one pD 2.5 solution 225 mM in U(VI) and 450 mM in CA, and four sample solutions with 100 mM CA and either 50 or 100 mM U(VI) for both pD 2.5 and 5, respectively. The sample using $^{17}OH_2$ was prepared by adding 500 µl of a D_2O solution 125 mM each in uranyl nitrate hexahydrate (VWR, > 99%) and trisodium citrate (Roth, *p.a.*) to 500 µl $^{17}OH_2$ (Eurisotop, 10% ^{17}O) prior to carefully adjusting to pD 7.0 (NaOD). This yielded 1 ml of a solution finally containing 61 mM uranyl(VI) citrate and 5% ^{17}O-enriched water. *UV-Vis studies* cover a titration series for pH 2–9, with 0.5 mM U(VI) and 10 mM CA, in 100 mM $NaClO_4$ solution. *ATR FT-IR samples* were prepared in a glovebox under N_2 atmosphere, comprising aqueous solutions in the pH range 2–9, 10 mM each in U(VI) and CA, containing 100 mM NaCl for ionic strength maintenance. *EXAFS samples* of 50 mM U(VI) and 500 mM CA, at pH values of 4 and 7, respectively, were filled in polyethylene pipette reservoirs that were subsequently heat-sealed.[39]

Methods

NMR spectroscopy. ^1H and broadband-decoupled ^{13}C spectra were measured on a Varian Unity Inova 400 9.4 T spectrometer, using a 5 mm direct detection broadband probe. ^1H NMR spectra were in part acquired with water signal suppression by a 2 s pre-saturation pulse with offset on the HDO resonance. ^1H and ^{13}C spectra were referenced relative to the $Si(Me)_3$ signal of TMSP with δ_H and δ_C set to 0 ppm. Temperature-dependent (VT) ^{13}C NMR as well as ^{17}O NMR measurements were performed on an Agilent DD2-600 14.1 T system, utilizing a 5 mm oneNMR™ probe for VT-^{13}C NMR and the sample with 5% ^{17}O-enrichment, and a 10 mm broadband direct detection probe for the sample of natural ^{17}O abundance (0.038%), respectively. ^{17}O spectra were obtained using 0.05 s acquisition time, 0.2 s relaxation delay, and accumulating 67k and 381k transients,

respectively. The bulk water signal was used as reference (δ_O 0 ppm). The double-quantum-filtered H,H-correlation spectrum (DQF-COSY) for the pD 2.5 sample was acquired at a 11.7 T Bruker Avance III NMR spectrometer at 0 °C. *UV-Vis spectroscopy* was performed in the 350–700 nm spectral range by means of a flow-through set-up (Figure S1, Supporting information, SI), comprising the vessel containing the analyte and a Blue Line 16 pH-microelectrode (Schott Instruments) connected to a InoLab WTW 720 pH-meter, a magnetic and heating stirrer ($T = 25 \pm 1$ °C), a pump, and the spectrophotometer (Varian Cary 5G). The components were connected *via* silicone tubes (4 mm in diameter) conveying the analyte to a flow-through cuvette ($d = 1$ cm, quartz Suprasil®, Fisher Scientific). For baseline correction a 0.1 M $NaClO_4$ blank solution was used. *ATR FT-IR* difference spectra, *i.e.*, subtraction of the blank (CA only) solution, were measured in the range between 3900 and 400 cm^{-1} on a Bruker Vertex 70/v spectrometer equipped with a liquid-nitrogen cooled mercury cadmium telluride (MCT) detector by accumulating 128 scans, using the OPUS™ software for data acquisition and evaluation. The used ATR accessory was a horizontal diamond crystal with 9 internal reflections (DURA SamplIR II, Smiths Inc.). The ATR cell was purged with a current of dry N_2 (dew point < 213 K), and flushed with de-ionized water between measurements of the respective solutions. *EXAFS spectroscopy.* U L_{III}-edge X-ray absorption spectra were measured in transmission mode[39] at the Rossendorf Beamline (ROBL), ESRF, Grenoble, France.[40] For energy calibration, an yttrium foil was measured in transmission mode. The program suite EXAFSPAK[41] was used for the data treatment, *i.e.*, energy calibration, averaging of multiple sample scans, isolation of the EXAFS signal, and data fitting. The photoelectric ionization potential (E_0) was fixed at 17.185 keV for all spectra. *DFT calculations* were performed in aqueous phase using Gaussian 09 program[42] utilizing the DFT method (B3LYP[43, 44]) through the use of the conductor-like polarizable continuum model (CPCM).[45, 46] The energy-consistent small-core effective core potential (ECP) and the corresponding basis set suggested by Dolg *et al*.[47] were used for uranium. The most diffuse basis functions on uranium with the exponent 0.005 (all s, p, d, and f type functions) were omitted as in previous studies.[48] For C, O, and H valence double-zeta plus polarization basis was used.[49] The Gibbs energy correction to the electronic energy was calculated at the same level from the vibrational energy levels in aqueous phase and the molecular partition functions. Structures were confirmed to be at their energy minima through vibrational frequency analysis where no imaginary frequency was found to be present. Spin–orbit effect and basis set superposition error (BSSE)

corrections were neglected. *Stability constant determination.* UV-Vis and ATR FT-IR single-component spectra and stability constants together with their concentration distribution were calculated employing the multivariate factor analysis program SPECFIT/32.[50] This program works on the basis of a principle components analysis by single value decomposition of the spectral mixtures and a nonlinear regression aimed to minimize chi-square between measured spectra and their reproductions by the Levenberg–Marquardt method. Thereby, sample conditions (pH, concentrations, ionic strength, temperature, protonation constants of the ligand, according to Hummel *et al.*[16] and Silva *et al.*[51]) and well as the reaction equation and the corresponding law of mass action are used as input parameters.[52] Formation constants, β, of uranyl(VI) citrate complexes are calculated from the law of mass action according to the reactions stated in Eqns. (1) through (5).

RESULTS AND DISCUSSION

Uranyl(VI)-citric acid binary dimeric complexes

Remarkably, literature dealing with aqueous uranyl(VI) citrate speciation or molecular structures respects only poorly that a chiral center is induced in the ligand due to complexation. The resulting complexes exhibit different configurations of their asymmetric carbons and ultimately form spectroscopically different isomers. Although the site exchange for the 'terminal' C1/C5 carboxyl groups is known, a configuration change at the central carbon (C3) is not considered in this process.

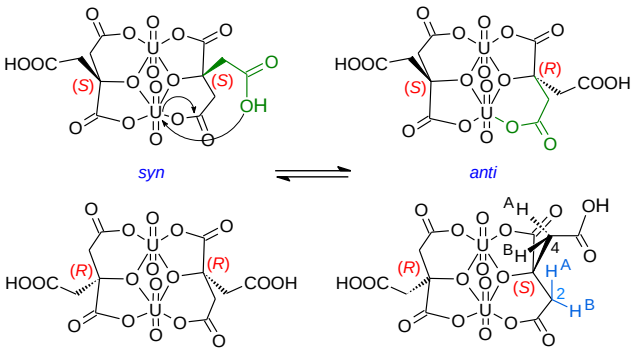

Figure 2. Generic configuration change exemplarily shown for the 2:2:0 complex upon intramolecular site exchange together with configurations of the chiral carbon atoms. The resulting

two diastereomeric pairs of enantiomers are denoted *syn* and *anti*, according to the relative position of the unbound -CH_2COOH moieties, *i.e.*, on the same side or on opposite sides of the molecular plane, respectively; coordinating water is omitted for clarity.

Figure 2 shows a generic example of intramolecular site exchange and concomitant configuration change of the respective asymmetric carbon (C3), whereby the given initial arrangement is *syn*, that is both unbound -CH_2COOH moieties are on the same side of the molecular plane, corresponding to the same configuration, here (*S*,*S*) for either ligand's chiral center. During intramolecular exchange between coordinating -CH_2COO–U(VI) and unbound -CH_2COOH, the configuration in the concerning asymmetric carbon changes. Subsequently, both -CH_2COOH moieties are *anti*, now on opposite sides and the chiral centers of opposite configuration (*S*,*R*). Corresponding enantiomers (*R*,*R*) and (*R*,*S*) are shown in Figure 2 (bottom), finally yielding two diastereomeric pairs of enantiomers. Hence, two forms of the $(UO_2)_2(HCit_{-H})_2^{2-}$ species, hereafter denoted *syn*- and *anti*-isomer, are spectroscopically distinct.

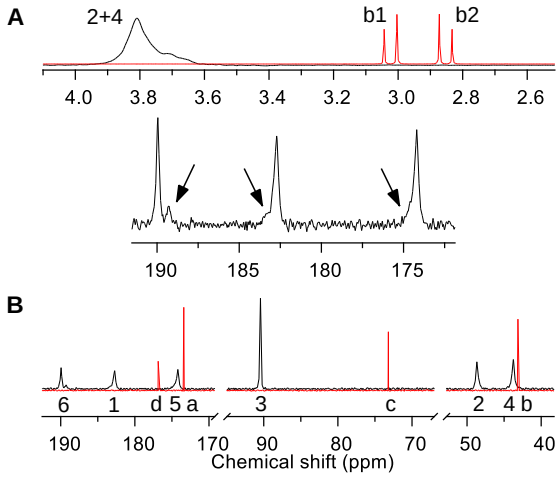

Figure 3. ^{1}H (A) and $^{13}C\{^{1}H\}$ NMR spectra (B, expansion as inset) at 25 °C of pD 2.5 D_2O solutions 250 mM in CA only (blank solution, red spectra), and in the presence of 250 mM U(VI) (black spectra). Arrows indicate the (in part obscured) secondary signals.

The spectra in Figure 3 feature U(VI)-bound CA exclusively of $(UO_2)_2(HCit_{-H})_2^{2-}$ as the chosen sample conditions ensure formation of the (binary) dimeric complex only. In principle, the complex signals are considerably shifted downfield as compared to the unbound ligand. The occurrence of monomeric complexes such as 1:1 or 1:2 species conceivably appearing in the sample is excluded due to observation of only one C3 associated signal in the characteristic 70–100 ppm range. U(VI) complexation-induced ^{13}C chemical shift changes, $\Delta\delta_C$ (relative to free ligand), are in line with Nunes and Gil[24] and are thus reported with Table S1, SI. In fact, the magnifications in Figure 3 (and Figure S3, SI) reveal a set of secondary signals (indicated by arrows) which are partially resolved and partially overlap with the main signals, resulting in occasionally broadened or distorted signal bases. These sets of main and secondary signals are assigned to the predominant and the less preferred isomer, respectively. Nunes and Gil[24] already concluded that the five-membered ring fragment involving the central carboxyl group (C6) is retained, while the terminal carboxyl groups (C1/C5) show rapid site exchange. Exactly for this reason for both isomers the carbon signals of the central carboxyl group (C6) are well resolved (190.0 and 189.3 ppm, respectively, insets in Figure 3, and Figure S3, SI), while the secondary signals, especially those of the -CH_2COO carbons, can hardly be observed when averaging with the main signals of the predominant isomer. The narrow C3 signal indicates this site to be fixed within the structures and to be remote to the exchanging sites. Although two different isomers can be observed, up to this point no decision can be made which set of signals attributes to which isomer.

The DQF-COSY spectrum (Figure 4) obtained at 0 °C discloses the correlations within the distinct methylene groups. The four particular ^1H signals A through D, each of which being a doublet owing to geminal coupling, belong to the two pairs of diastereotopic hydrogens within one CA ligand as labeled in Figure 2, bottom right. Deconvolution of the projected ^1H NMR spectrum reveals the individual $(UO_2)_2(HCit_{-H})_2^{2-}$ complex signals. Discrimination between corresponding protons for the individual isomers is not feasible under these conditions.

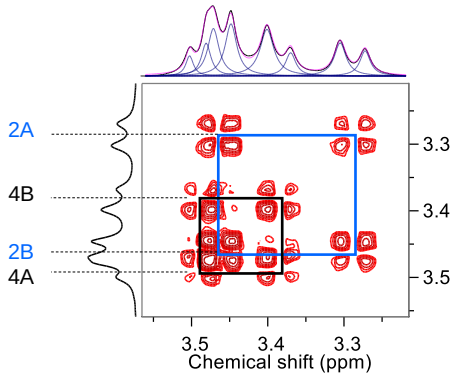

Figure 4. DQF-COSY of 50 mM U(VI) and 100 mM CA pD 2.5 D_2O solution at 0 °C, with the correlating signals indicated. The horizontal projection shows the 1D-^{1}H spectrum together with signal deconvolution.

^{1}H NMR spectra acquired at 25 and 0 °C for both pD 2.5 and 5 of solutions either 50 or 100 mM in U(VI) and 100 mM in CA, respectively, are shown in Figure S2, SI. At 25 °C, the overlapping ^{1}H signals of the $(UO_2)_2(HCit_{-H})_2^{2-}$ complex give an unresolved feature, *cf.* Figure 3A. Sample cooling improves resolution upon signal separation as isomerization slows down. Signal separation at low temperature evinces the dependency of the isomerization rate on the sample conditions. Increasing U(VI) concentration or especially pH causes the speciation to shift from the exclusive existence of $(UO_2)_2(HCit_{-H})_2^{2-}$ towards the coexistence of the former and the ternary $(UO_2)_2(HCit_{-H})_2(OH)^{3-}$ species (*vide infra*), reducing spectral resolution as their signals overlap (Figure S2, SI).

A series of temperature-dependent ^{13}C NMR spectra was recorded for a pD 2.5 solution 225 mM in U(VI) and 450 mM in CA, whereby excess of the latter warrants that all U(VI) is complexed. ^{13}C NMR reveals a much better signal separation for the isomers and hence allows for determination of the rates and, consequently, activation energy, E_a, for the isomerization. For detailed spectra and calculation, refer to Figure S3, SI. Briefly, based on the line width of the complex's signal compared to that of the internal reference (acetonitrile) the exchange rate at −6 °C amounts to about 30 s^{-1}. At 60 °C the C6 signals coalesced, corresponding to a rate of about 249 s^{-1}. According to the Arrhenius equation, E_a is calculated to be 24 kJ mol^{-1}.

^{17}O NMR spectroscopy finally allowed a definitive assignment of the two distinct sets of signals already observed in ^{1}H and ^{13}C NMR spectra. Owing to chemical and spectroscopic characteristics, at natural ^{17}O abundance signals of interest could only be obtained from O_{yl}. From literature no simple correlation of complexation-induced $^{17}O_{yl}$ spectral effects is discernable, as is known for, *e.g.*, the systematic weakening of O_{yl}–U–O_{yl} bonds as associated with bathochromic shifts of uranyl's symmetric (ν_1) and antisymmetric (ν_3) stretching vibrations in Raman and IR spectra, respectively, upon its coordination by (in)organic ligands.[48, 53, 54]

The O_{yl} ^{17}O NMR spectrum in Figure 5 corresponds to the same sample solution as the ^{1}H and ^{13}C spectra in Figure 3. As ascertained from the latter, all ligand is bound in the $(UO_2)_2(HCit_{-H})_2^{2-}$ complex. Apart from the small fraction of free UO_2^{2+} (δ_O 1114 ppm), again two sets of signals are detected, comprising two main and four secondary signals. DFT calculation of structures and corresponding δ_O values (Table 1) for both isomers unambiguously correlates main signals with *syn* isomer and secondary signals with *anti* isomer. The *syn* isomer is basically of C_2 symmetry. With a C_2 rotational axis and both unbound -CH_2COOH moieties located on the same side of the molecular plane one O_{yl} is *cis* while the other O_{yl} of the same uranyl entity is *trans* to these moieties. Thus, each pair of O_{yl} on either side of the molecular plane gives rise to one ^{17}O resonance whereupon two signals of equal intensity occur. The uranyl entities are thus best characterized and designated as $O_{yl,A}$–U–$O_{yl,B}$, *cf*. Figure 5 (inset) and Figure S4, SI.

DFT-calculated complex solution structures show that the *anti* isomer is distorted to such an extent that the overall symmetry reduces from expected C_i to actual C_1 (Figure S4, SI). As a result, all four O_{yl} are unique and thus give rise to different resonances that correspond to the four secondary signals observed. Although (for both isomers) the calculated δ_O values are overestimated by 32 ppm at most, they agree very well with the relative resonance frequency differences observed in the experiment (Table 1). DFT-calculation reveals that one six-membered ring fragment is remarkably twisted and that the enclosed UO_2 (U2 in Figure S4, SI) shows a substantial deviation from pentagonal bipyramidal coordination. The two O_{yl} of that particular U2 disclose the two largest calculated δ_O, (2A/2B) while the O_{yl} of the other uranyl unit (U1) featuring an almost regular coordination polyhedron reveal both the closest and lowest δ_O values overall (1A/1B).

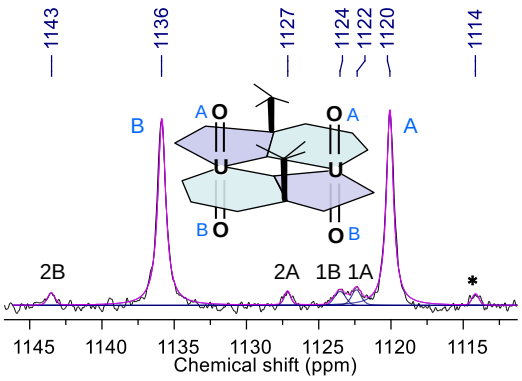

Figure 5. O_{yl} region of the ^{17}O NMR spectrum obtained from a pD 2.5 D_2O solution 250 mM each in U(VI) and CA at natural ^{17}O abundance. The main signals are assigned to the corresponding sites in the sketched $(UO_2)_2(HCit_{-H})_2^{2-}$ *syn* isomer's structure (inset), the secondary signals are assigned to the *anti* isomer, and the signal of free uranyl(VI) ion is indicated by an asterisk.

Table 1. Comparison of spectroscopically observed and DFT-calculated ^{17}O chemical shifts (ppm) of O_{yl} in the two isomers of the $(UO_2)_2(HCit_{-H})_2^{2-}$ complex.

	syn		*anti*			
site	A	B	1A	1B	2A	2B
observed	1120	1136	1122	1124	1127	1143
calculated	1135	1157	1142	1143	1159	1168

Uranyl(VI)-citric acid ternary dimeric complexes

UV-Vis spectroscopy reveals that for excess CA even in pH 2 solution U(VI) is complexed, forming $(UO_2)_2(HCit_{-H})_2^{2-}$, corresponding to the red spectrum in Figure 6 (top). Above pH ≈ 4, the spectra show a slight bathochromic shift of and increasing molar absorptivity at the absorption maximum $\lambda(\varepsilon_{max})$, inset in Figure 6, as also described by, *e.g.*, Berto *et al.*[28] The normalized single-component UV-Vis spectra exhibit the same $\Delta\varepsilon_{max}$ increments for consecutive species, *viz.* 48 M^{-1} cm^{-1} in $NaClO_4$ media, *cf.* Figure 6, top. The UV-Vis spectra obtained by Berto *et al.*[28] for

solutions containing KNO_3 as supporting electrolyte reveal the same principal spectral behavior, with $\Delta\varepsilon_{max}$ increments of 26 M^{-1} cm^{-1}. Differences in the absolute values are ascribed to the different background electrolytes used for ionic strength maintenance.[28] Further details are stated with Table S2 in the SI.

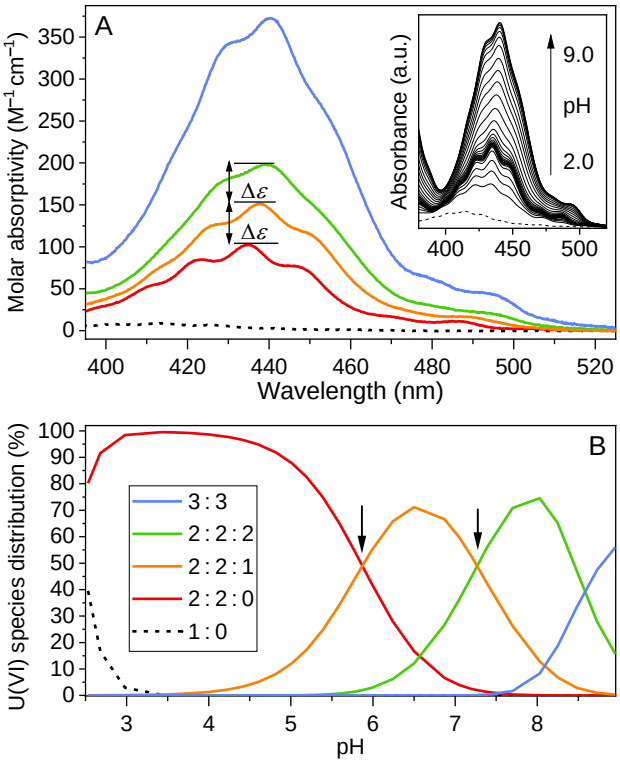

Figure 6. Single-component spectra (A) obtained from a UV-Vis spectrophotometric pH 2–9 series 0.5 mM in U(VI), 10 mM in CA, and 0.1 M in $NaClO_4$ (inset). (B) U(VI) species distribution relative to total U(VI) calculated from the determined stability constants given in Table 2 using the solution composition as for the experiment in (A).

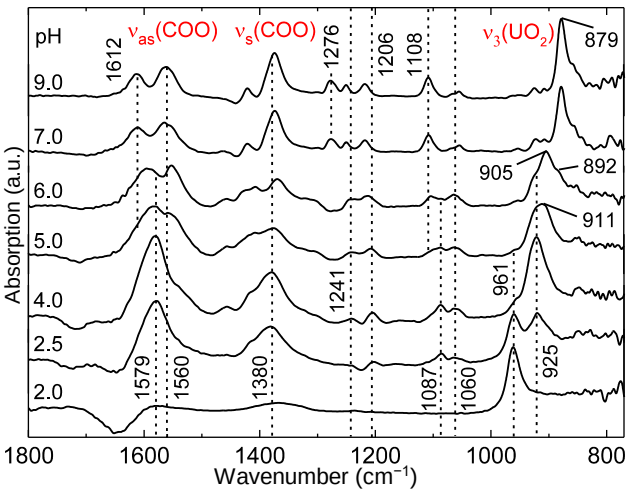

Figure 7. ATR FT-IR difference spectra of a pH-titration series pH 2–9 under N_2 atmosphere, with pH values stated with the spectra, for aqueous solutions containing 10 mM U(VI), 10 mM CA, and 0.1 M NaCl. Note the indicated features of interest, with numerals referring to wavenumbers in cm^{-1}.

ATR FT-IR difference spectra depict absorptions of the formed complexes only, since the free ligand spectrum is subtracted (Figure 7, and for pH-dependent spectra of the ligand see Figure S5, SI). The spectrum obtained at pH 2 is dominated by the $\nu_3(UO_2)$ of the uranyl aquo-ion at 961 cm^{-1}. At pH 2.5 the $\nu_3(UO_2)$ observed at 925 cm^{-1}, as well as the symmetric and antisymmetric stretching vibrations of the carboxylate groups, ν_s(COO) and ν_{as}(COO), found at about 1380 and 1560–1580 cm^{-1}, respectively, indicate the formation of $(UO_2)_2(HCit_{-H})_2^{2-}$ and agree well with reported values of 919, 1382, and 1579 cm^{-1}, respectively.[26] In line with UV-Vis measurements, increasing pH results in the appearance of new absorptions which exhibit a successive bathochromic shift of $\nu_3(UO_2)$, with corresponding values determined as 911 and 905 cm^{-1}, respectively. Spectral deconvolution (Figure S6, SI) allowed a tentative assignment of the individual absorption bands related to the dimeric and trimeric U(VI)-CA complexes.

Based on the $(UO_2)_2(HCit_{-H})_2^{2-}$ species, two sequences for structural changes in the complexes are conceivable, that is, deprotonation of the unbound -CH_2COOH residues, Eqn. (6), or deprotonation of the U(VI)-coordinating water ligands, Eqn. (7); *cf.* Figure 1B.

$$(UO_2)_2(HCit_{-H})_2(H_2O)_2^{2-} \rightarrow (UO_2)_2(HCit_{-H})(Cit_{-H})(H_2O)_2^{3-} \rightarrow (UO_2)_2(Cit_{-H})_2(H_2O)_2^{4-} \quad (6)$$

$$(UO_2)_2(HCit_{-H})_2(H_2O)_2^{2-} \rightarrow (UO_2)_2(HCit_{-H})_2(OH)(H_2O)^{3-} \rightarrow (UO_2)_2(HCit_{-H})_2(OH)_2^{4-} \quad (7)$$

Both spectroscopies refer to features directly correlated with uranyl(VI). In case of IR, the uranyl(VI) entities show a decrease in their antisymmetric stretching vibration frequency, $\nu_3(UO_2)$. The incremented increase in absorptivity in ligand-to-metal charge-transfer (LMCT) transitions observed in the UV-Vis spectra essentially refer to the uranyl(VI) as the chromophore. If, for instance, changing the complexes' overall symmetry was the reason (as is the case in either sequence), then ε_{max} should at first increase upon reducing the complex' symmetry, but as the higher symmetry (same overall symmetry elements as for the initial species) is restored, ε_{max} should then (re-)decrease.

Changes in the unbound -CH_2COOH residues, *i.e*. deprotonation upon increasing pH, is too remote to affect the spectral features associated with U(VI). By contrast, the structural changes occurring in direct vicinity of the UO_2 entities upon deprotonation of the uranyl(VI)-coordinating water, *i.e.* hydrolysis *within* the binary U(VI)-CA dimeric complex according to U-OH*H* → U-OH + H^+ (see coordinating H_2O in Figure 1B), much better explain the observations in the IR and UV-Vis spectra. Taking together our spectroscopic findings, and the titrimetric/potentiometric and spectrophotometric results by others,[20, 21, 28] we conclude that the ternary dimeric U(VI)-CA 2:2:1 and 2:2:2 complexes refer to $(UO_2)_2(HCit_{-H})_2(OH)(H_2O)^{3-}$ and $(UO_2)_2(HCit_{-H})_2(OH)_2^{4-}$, respectively.

Correspondingly, the intercepts of the curves describing the individual dimeric complexes in the speciation diagram (*cf*. Figure 6, bottom) represent apparent pK_a values for the dissociation of the coordinating water molecules, determined as 5.9 and 7.3 (indicated by solid arrows). The latter are somewhat higher than the pK_a value of the bare $UO_2(H_2O)_5^{2+}$ reported as 5.24 ± 0.25.[55] This is because H^+ abstraction is impeded owing to both the considerably decreased Lewis acidity of the uranyl(VI) entities upon complexation by the stronger Lewis base citrate (compared to the weaker base water) and the increased overall anionic charge.

Table 2. Stability constants for aqueous dimeric and trimeric U(VI)-CA species.

species	log β^a			method
	this work	Ref. 28[b]	Ref. 28[c]	

2:2:0	19.7 ± 0.1[d]	19.50 ± 0.01	19.26 ± 0.02	UV-Vis
	19.3 ± 0.2[b]	—	—	ATR FT-IR
2:2:1	13.8 ± 0.1[d]	14.02 ± 0.02	14.05 ± 0.03	UV-Vis
	14.2 ± 0.3[b]	—	—	ATR FT-IR
2:2:2	6.5 ± 0.1[d]	8.22 ± 0.02	8.87 ± 0.01	UV-Vis
3:3	−(5.4 ± 0.2)[d]	—	—	UV-Vis
3:2	—	−(2.03 ± 0.06)	−(0.92 ± 0.03)	UV-Vis
	−(1.0 ± 0.5)[b]	—	—	ATR FT-IR

[a] ± standard deviation; [b] 0.1 M NaCl; [c] 0.1 M KNO_3; [d] 0.1 M $NaClO_4$

Stability constants (log β) calculated with SPECFIT/32[50] from ATR FT-IR and UV-Vis spectra are summarized in Table 2, and are in good agreement with literature. Only the 2:2:2 species yielded a somewhat smaller value. Since the vibration frequencies of the ternary dimeric species are very similar and thus give rise to broad, hardly resolved bands, log β of the latter could not be calculated from IR spectra.

To illustrate the effects of the described species, a representative example from uranium-contaminated areas of the South African gold mining district ([U(VI)] = 3×10^{-7} M; field data taken from Winde *et al.*,[56] with addition of 1×10^{-5} M citric acid) was used to compute species distribution for different boundary conditions, see Figures S7–S9 (SI) for the results.

Additionally, Figure S10 shows the aquatic speciation of 1×10^{-4} M U(VI) and 1×10^{-2} M CA in 0.1 M NaCl medium at 25 °C under ambient atmosphere, once without and once including the ternary dimeric species (2:2:1 and 2:2:2) as well as the trimeric (3:3 and 3:2) species in the calculation. The graph nicely reflects the findings from the different spectroscopies regarding emergence and coexistence of the ternary species as well as the predominance of the 3:2 species as of circumneutral pH and its existence over a large pH range.

Uranyl(VI)-citric acid trimeric complexes

In the 3:3 and 3:2 trimeric species, the ligand is completely deprotonated (Cit_{-H}^{4-}), according to $(UO_2)_3(\mu_3\text{-}O)(Cit_{-H})_3^{8-}$ and $(UO_2)_3(\mu_3\text{-}O)(\mu_2\text{-}OH)(Cit_{-H})_2^{5-}$.[17, 18] The samples' speciation, *i.e.*, predominance of either trimeric species, can be well adjusted by the sample conditions.[17, 18, 28] Circumneutral pH and excess CA strongly favor the 3:3 species whereas both high pH values and excess U(VI) favor the 3:2 species, and the respective 6:6 and 9:6 superstructures are favored especially at high overall concentrations.

As of pH 5 the $\nu_3(UO_2)$ modes associated with the trimeric species appear in the ATR FT-IR. Owing to the sample conditions the 6:6 sandwich complex forms. Corresponding features appear rather weak, hence spotted only by deconvolution and, in the pH 6 spectrum, as a shoulder at 892 cm^{-1} while above pH 6 the 3:2 species predominates, giving rise to the band at 879 cm^{-1} (Figure 7).[18] With the aid of DFT-calculated molecular vibration frequencies, the signals at 1060 and 1087 cm^{-1} can be assigned to combination vibrations of C3–O stretch and H–C–H twist, as well as H_2C–C3 stretch and H_2C–C3–CH_2 bend, respectively associated with the complexes' five- and six-ring fragments. Analogously, the 1206 and 1241 cm^{-1} modes have contributions from vibrations related to the carbon framework as well as stretching and deformation modes in the OC–O and H_2C–COO fragments. Above pH 6, a band at 1276 cm^{-1} appears, that at 1087 cm^{-1} shifts towards higher frequencies, and $\nu_{as}(COO)$ is split into two modes, among which one emerges at 1612 cm^{-1}. The latter findings are ascribed to the changed binding situation in the 3:2 species, *i.e.*, increased complex' U(VI):CA ratio, μ_2-OH bridged uranyl(VI) units concomitantly decreasing their Lewis acidity as well as reduced overall symmetry.

By means of the applied sample conditions, 3:3 and 3:2 species' log β values could be calculated from UV-Vis and ATR FT-IR spectra, respectively (Table 2). Although the errors are in principle somewhat larger for the IR-based stability constants, the 3:2 log β value fits well within the range of reported values. The stability constant of the 3:3 species is unprecedented; extrapolation to infinite dilution, applying the Davies equation,[57] gave $\log \beta^\circ = -(8.6 \pm 0.2)$; for $\log \beta^\circ$ of the other complexes, see Table S3, SI.

The high solubility of and the lacking dynamics within the 6:6 uranyl(VI) citrate sandwich complex are ideal prerequisites for intense and sharp NMR signals and were exploited to detect the ^{17}O NMR signal of the trinuclear uranyl(VI) core bridging μ_3-oxygen. Under suitable conditions the sample solution contains almost exclusively the 6:6 Na^+ sandwich complex,[17]

allowing for straightforward signal assignment. A corresponding sample was prepared adding ^{17}O-enriched water prior to pD adjustment.

Since the O_{yl} are inert and show no isotopic exchange under the applied conditions, only oxygen in hydrolytic water is isotopically labeled. Thus, upon increasing pD, hydrolysis in U(VI)-coordinating HD^{17}O causes isotopic labeling of the μ_3-O *in situ*, resulting in the first observation at δ_O 583 ppm (Figure 8), comparable to μ_3-^{17}O signals in poly-oxo anions of Mo (516 ppm)[58] and Ti (575–527 ppm)[59]. For comparison, the line widths are 460, 140, and 90 Hz of the signals respectively associated with μ_3-O, NO_3^-, and HDO.

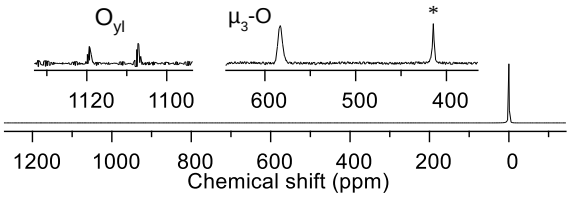

Figure 8. ^{17}O NMR spectrum of a pD 7 sample 61 mM each in uranyl(VI) nitrate and trisodium citrate containing 5% ^{17}O-enriched water, showing signals associated with the uranyl(VI)-citrate 6:6 Na^+ sandwich complex. The ^{17}O signal of the nitrate anion (414 ppm relative to water at 0 ppm) is marked by an asterisk.

In addition, the 6:6 complex was investigated by EXAFS spectroscopy, whereby the obtained distances (Table 3) refer to the shell fits within the sandwich complex constituting 3:3 U(VI)-CA species. The raw U L_{III}-edge k^3-weighted EXAFS data, corresponding Fourier-transforms and model structures as used for the shell fit together with structure parameters are provided with Figure S11 and Table S4, SI. The symmetric 3:3 species (Figure 1C) is characterized by a bridging μ_3-O as unambiguously revealed by X-ray crystallography in single-crystals[18] and by ^{17}O NMR in solution shown above, with the μ_3-O–U distance fitted to 2.20(2) Å. In this context, the key issue is the discrimination between features of the μ_3-O and the other equatorial oxygen atoms. Accordingly, the radial particle distribution function (RPDF) was calculated, providing a density function of interatomic distances. The Landweber iteration approach is thereby used to reconstruct asymmetric RPDFs from the EXAFS spectrum.[39, 60]

Similar to corresponding uranyl(VI) hydrolysis species,[61] due to oligomerization from 2:2 to 3:3 complex, the U–U distances shorten from 3.903(6) to 3.801(3) Å. Owing to the μ_3-O, the 3:3

complex is tightened in its radial dimension, whereupon in the single-crystal structures the U–U distances decrease from 3.890 to 3.762(14) Å when going from 2:2 to 3:3 complex, and the latter showing a μ_3-O–U distance of 2.231(15) Å.[18] Notably, unlike the 2:2 and the 3:2 complexes, the 3:3 complex possesses no water ligands as the coordination around the uranyl(VI) entities is saturated by the citrate ligands and the μ_3-O. Additionally, the O_{yl}–U–O_{yl} bond lengths significantly increase to 1.806(1) Å.

Table 3. Interatomic distances in Å[a] associated with U(VI)-CA 2:2 species as well as 3:3 species in 6:6 Na^+ sandwich complex.

	2:2 species			3:3 species	
	Ref. 39[b]	Ref. 25[c]	Ref. 18[d]	Ref. 39[b]	Ref. 18[d]
U–O_{yl}	1.784(1)	1.78(2)	1.779(5)	1.806(1)	1.798(9)
U–O_{eq}	2.364(3)	2.38(2)	2.380(44)	2.373(9)	2.366(26)
U–U	3.903(6)	3.93(2)	3.890	3.801(3)	3.762(14)
μ_3-O–U	—	—	—	2.20(2)	2.231(15)

[a] uncertainty given in parentheses as last digit(s); [b] EXAFS, solution structures; [c] EXAFS (0.04 M U(VI), 0.1 M CA, pH 3.8); [d] single-crystal X-ray diffraction; data according to CCDC nos. 1031410 and 1031412.

Upon increasing pD, the complexes with U(VI):CA ratio equal to unity are displaced by species with U(VI):CA ratio of 1.5:1 which can be seen as the replacement of citrate by OH^- as ligand. A pD 7.5 solution initially equimolar in both U(VI) and CA thus exhibits free citrate. ^1H and ^{13}C NMR spectra in Figures 9A and B, respectively, disclose three sets of signals, owing to the sample conditions, associated with the 6:6 U(VI)-citrate Na^+ sandwich complex, 9:6 U(VI)-citrate macrocycle (circles), and free citrate.

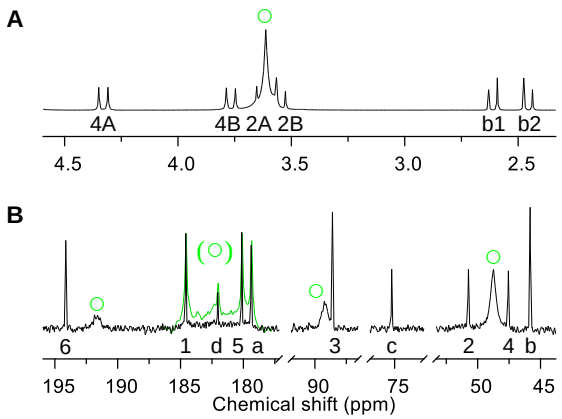

Figure 9. ^{1}H (A) and ^{13}C{^{1}H} (B) NMR spectra of 250 mM U(VI) and 250 mM CA in D_2O at pD 7.5. Note the overlaid part with line broadening factor lb = 15 Hz (green). Signals associated with the 9:6 complex are indicated by green circles; other signals assigned according to labeling in Figure 1.

Since the 6:6 sandwich complex is lacking any dynamics, its ^{1}H and ^{13}C NMR signals are well resolved. In contrast, the signals of the 9:6 complex (and its sub-units) show remarkable broadening upon spectral averaging caused by dynamic processes. Especially those of the terminal carboxylates (C1/C5), as the reactive sites, are broadened to such an extent that they hardly differentiate from the baseline. As described for the dimeric species (*vide infra*), coordinating and unbound -CH_2COO moieties are subject to mutual intramolecular site exchange. Additionally, intermolecular reactions comprise association and dissociation among the sub-units and the 9:6 macrocycle.

From ^{13}C NMR, Figure 9B, it can be concluded that the dynamic reaction equilibrium is shifted towards the 9:6 superstructure. The macrocycle's $\Delta\delta_C$ of carboxyl C6 as well as of the U(VI)-bound -CH_2COO moieties' C1/C2 are somewhat smaller as compared to those of the 6:6 complex since in the 9:6 complex the respective uranyl units' Lewis acidity is decreased upon μ_2-OH bridging. However, pertaining to the carbons C4/C5, $\Delta\delta_C$ is larger for the 9:6 than for 6:6 complex, since the corresponding -CH_2COO moieties are unbound in the sandwich complex while in the 9:6 complex they are bridging the constituting 3:2 sub-units. Therefore, in the macrocycle all C3-bound residues are involved in U(VI)-coordination causing additional electron density withdrawal

and, possibly, some torsional strain, resulting in $\Delta\delta_C$ larger for C3 in the 9:6 than in the 6:6 molecule.

For each single hydrolysis step or, in general, for any (additional) Lewis base coordination, the metal's Lewis acidity (successively) decreases since the uranyl(VI) entity withdraws electron density. Accordingly, ligand-to-metal charge transfer (LMCT, O_{eq}–U) bands in UV-Vis absorption spectra are red-shifted and the U–O_{yl} bond force constants and, hence, the vibration frequencies are decreased as observed by vibrational spectroscopies.[48, 54, 61-65] Correspondingly, since the chemical shift is a measure for the electron density, the reduced U(VI) Lewis acidity results in smaller electron density withdrawal and thus smaller $\Delta\delta_C$. The latter fact is consistent with theoretical studies for ternary model systems,[66, 67] and the observed bathochromic shift of UO_2 ν_1 and ν_3 upon changing speciation from dimeric to trimeric U(VI)-CA complexes as shown in Figure 7 and elsewhere.[18, 26] For $\Delta\delta_C$ values refer to the considerations stated with Figures S12 and S13, SI, showing corresponding H,C-HMBC and H,H-COSY pD 7.5 spectra.

CONCLUSIONS AND OUTLOOK

Although already investigated for decades, the results of this unique multi-method approach allowed deeper fundamental insights into the structures of the formed uranium(VI)-CA complexes on a molecular level. Presented complex species and structures are consonant among all applied complementary spectroscopic methods and supported by quantum chemical calculations. This work delivers a topical and reliable comprehension of dimeric and trimeric U(VI)-CA species in aqueous solution forming in acidic up to slightly alkaline media.

The objectives (i) to (iv) introduced in the *Motivation* section were achieved as follows.

First of all, we appreciate and build upon all the previous work dealing with this challenging system. With reference to issue (i), by outlining the progress in U(VI)-CA complex structure elucidation we addressed the major misconceptions leading to erroneous molecular structures. In this regard, we want to stress that *hydrolysis* is the consequence of strong polarization of the H<O>H bonds in water coordinating metal ions. Then, hydrolysis occurring already in strongly acidic media is caused by the metal ion's Lewis acidity. Accordingly, hydrolysis of U^{4+}, as a significantly stronger acid, happens even at pH < 1.[68, 69]

A repeatedly arising argument, and supposedly a misleading belief in previously proposed U-CA complex structures, is that strong complexing, *i.e.*, polydentate (chelating) ligands prevent U(VI) hydrolysis and formation of polynuclear species. The U(VI)-CA system is a superb, but not the only example disproving this reasoning, see also considerations on issue (iv), below. Thus, any U(VI)-coordinating water in ever so stable complexes is susceptible to hydrolysis even in strong acidic media as consequence of the interplay between metal ion Lewis acidity and solution pH. For instance, the two $HCit_{-H}^{3-}$ ligands in the dimeric 2:2:0 complex do not prevent hydrolysis; as coordinating Lewis bases they merely decrease U(VI) Lewis acidity and, thus, increase the pH for which the water molecules in the remaining fifth coordination site finally hydrolyze. Subsequently, the mono- and bis-hydroxo U(VI)-CA species denoted 2:2:1 and 2:2:2 occur in solution as proven by UV-Vis and ATR FT-IR spectroscopies. Upon further increasing pH, we hypothesize that at some point the 2:2:2 species breaks down, the $HCit_{-H}^{3-}$ ligand is released thereby forming Cit^{3-}. The consecutively emerging 3:3 complex forms by reaction of the trinuclear uranyl(VI) hydrolysis species $(UO_2)_3(\mu_3\text{-}O)(OH)_3^+$ with three Cit^{3-} thereby (again) releasing the alcoholic hydroxyl proton to finally yield $(UO_2)_3(\mu_3\text{-}O)(Cit_{-H})_3^{8-}$. The computed speciation distributions imply that in general the U(VI) hydrolysis species are the precursors for the polynuclear U(VI)-CA complex species. That is, even for 100-fold CA excess no polynuclear species form as long as the U(VI) solution is sufficiently diluted, such as 10^{-7} M.

Concerning issue (ii), on crucial consideration of the stereocenters induced in the molecules upon citrate complexation, the overall configurations of the dimeric complex isomers, *viz*. *syn* and *anti*, were proven by spectroscopy in aqueous solution. It was the first evidence that the $(UO_2)_2(HCit_{-H})_2^{2-}$ complex strongly favors the *syn* configuration in aqueous media, with both isomers coexisting and mutually interconverting with rates of ~30 and ~249 s^{-1} at −6 and 60 °C, respectively, in acidic media, corresponding to an activation energy of about 24 kJ mol^{-1}. By all of the methods applied to the aqueous U(VI)-CA system in general, and investigating the 2:2 complex in particular, *i.e.*, UV-Vis,[70, 71] EXAFS,[25] as well as Raman, FT-IR, and ESI-MS,[18, 26] it is questionable if any would be able to discriminate between the two isomers since in both the two uranyl(VI) units possess the same pentagonal bipyramidal coordination geometry as well as number and type of nearest neighbor atoms. Finally, only the combination of NMR spectroscopy and DFT calculation allowed unambiguous decision on the overall configurations, with ^{17}O NMR signals attributed to the individual uranyl(VI)-oxygen atoms in both isomers.

Virtually all single-crystal X-ray structures containing the dimeric U(VI)-CA complex in any manner reveal *anti* configuration.[18, 34, 35, 37, 72] Notably, there is one crystal structure that reveals the *syn* configuration, obtained under hydrothermal conditions (180 °C), facilitated by a water molecule bridging the *syn* -CH_2COOH moieties via hydrogen bonding.[36] Apparently, the *anti* isomer crystallizes preferably owing to its higher symmetry which enables regular arrangement in the crystal lattice, thereby overcoming the distortions calculated (and reflected by ^{17}O NMR data) in the solution structure. The *syn* isomer can, hence, be considered more soluble. As a matter of fact, the predominance of the *syn* isomer in solution was hitherto unnoticed, demonstrating that, especially upon different physicochemical properties of the isomers, the solid phase does not necessarily reflect speciation and structures found in aqueous solution, underlining the importance of rigorous solution studies.

With reference to point (ii), the trimeric species exhibit versatile features regarding both structure and dynamics. The basic 3:3 and 3:2 species predominate at lower overall concentrations up to low-millimolar range, and are subject to pronounced intramolecular dynamics. As of millimolar solution, corresponding superstructures form upon (self-)association, either by sandwiching metal ions (M = Na^+, Ca^{2+}, La^{3+}) by two 3:3 species as a Lewis acid–base adduct with $U–O_{yl}→M$ motif,[17] or by trimerization, with the remaining -CH_2COO^- moieties intermolecularly linking the 3:2 sub-units to form a macrocycle.[18] While the latter undergoes break-down and build-up reactions among its sub-units, the sandwich arrangement is lacking any dynamics. For this reason, the ^{17}O NMR signal of the trinuclear uranyl(VI) core μ_3-bridging oxygen could be observed for the first time.

Pertaining to point (iii), stability constants were determined for all dimeric and trimeric complex species, some of which as duplicates using complementary methods. The thus obtained values agree very well among one another and corroborate those reported in the literature. The stability constant of the 3:3 species was determined for the first time, being $\log \beta° = -(8.6 \pm 0.2)$. Consequently, the more stable 3:2 complex and its stoichiometric self-associates form by cost of the former upon passing neutral pH through alkaline conditions. Since the 3:2 complex occurs preferentially at higher pH, its formation is likely to be caused by the veritable reaction of OH^- present in solution as the stronger Lewis base (nucleophile) successively replacing the weaker nucleophile citrate. This is clearly seen in the pD 7.5 NMR spectra (Figure 9) by observation of citrate released upon replacing complexes with 1:1 U:CA stoichiometry (here 6:6) by those with

1.5:1 U:CA ratio (mainly 9:6). U(VI)-binding to the remaining unbound -CH_2COO^- moieties combined with liberation of coordinating water molecules from U(VI) (*cf*. Figure 1D) are additional enthalpic and entropic driving forces.

When U(VI) concentrations are as low as 10^{-7} M (µg/L range), only the mononuclear 1:1 species play a role. If one considers that as of U(VI) concentrations of 5×10^{-5} M and excess ligand the formed U(VI)-CA complexes are polynuclear,[27] in some technology-affected natural environments (issue of TENORM – technologically enhanced naturally occurring radioactive materials) both U(VI) and (organic) ligand concentration likely increase up to values allowing for formation of polynuclear complex species. However, these complexes are still rather weak compared to competing inorganic uranium(VI) complexes, namely hydroxides, carbonates and hydroxycarbonates. Consequently, species distribution calculations suggest that the characterized polynuclear uranium(VI)-citric acid species do not significantly increase uranium(VI) mobility in the environment; from a safety and risk assessment point of view, this is good news.

As regards point (iv), in both solid and aqueous phase uranium adopts the same structural 'core' features, *i.e*., $(UO_2)_2(\mu_2\text{-}OR)_2$ and $(UO_2)_3(\mu_3\text{-}O)(\mu_2\text{-}OR)_3$, with R being organic residues or H, the latter pertaining to the inorganic complexes $(UO_2)_2(OH)_2^{2+}$ ("2,2") and $(UO_2)_3(O)(OH)_3^+$ = $(UO_2)_3(OH)_5^+$ ("3,5") respectively, as shown by both X-ray based and optical methods as well as DFT calculation.[61, 63, 73-76] The organics comprise, for instance, besides citrate also lactate (Lac), malate (Mal), and tartrate (Tart). Related investigations[39] of U(VI) complexation by the latter three ligands (all performed at comparable sample conditions as for CA presented herein) are in very good agreement with the spectrophotometric data obtained by Feldman *et al*.[20] as well as the EXAFS fits for the respective dimeric complexes studied by Allen *et al*.[25] Corresponding $\lambda/\varepsilon_{max}$ values of 436/101, 435/102, and 433 nm/104 M^{-1} cm^{-1}, and U–U distances of 3.93(1), 3.930(7), and 3.932(6) Å are indicative of 2:2:0 dimeric species of U(VI) with Lac, Mal, and Tart, respectively. Moreover, $\lambda/\varepsilon_{max}$ as well U–U and μ_3-O–U distances determined to 440/344, 440/326, and 439 nm/340 M^{-1} cm^{-1}, as well as 3.814(2), 3.816(3), and 3.806(2) Å, and 2.19(1), 2.19(1), and 2.20(1) Å, are also very similar among one another and, with respect to the described citrate-related UV-Vis and EXAFS data (440 nm, 373 M^{-1} cm^{-1}, 3.801 and 2.20 Å), unambiguously evidence the analogous trimeric U(VI) complexes of Lac, Mal, and Tart, respectively.

Unruh *et al*.[77] published single-crystal X-ray structures for the trimeric uranyl(VI) complexes of Mal. Equimolar U(VI):Mal ratios resulted in the presence of 3:3 species in crystals obtained from

a pH 6 parent solution. At pH 7, however, only one pH unit above, the obtained crystals contain 3:2 species isostructural to those in the 3:2 U(VI)-citrate sub-unit (Figure 1D). Although not explicitly investigated, it is most likely that both these trimeric species were essentially present as aqueous complexes in their respective parent solutions. Since Mal possesses the same basic structure as CA, the tridentate U(VI)-binding fashion is in principle identical, but as the unbound -CH_2COO^- moiety is lacking, the 3:2 U(VI)–Mal species does not assemble as a 9:6 macrocycle but ligates to uranyl(VI) carbonate units instead.[77]

Obviously, even the 3:2 U(VI)-citrate and, accordingly, the 3:2 U(VI)–Mal structure can be correlated to a corresponding inorganic hydrolysis isostructure, *viz.* the $(UO_2)_3(O)(OH)_5^-$ = $(UO_2)_3(OH)_7^-$ ("3,7") complex (Figure S14, SI). Moreover, the structural similarities are not only restricted to α-hydroxy acids. Further evidence for complexes containing the $(UO_2)_3(\mu_3\text{-}O)(\mu_2\text{-}OR)_3$ 'core' structure is given by, *e.g.*, terephthalate,[78] *p*-nitrobenzoate,[79] and nucleotides,[80] with the latter containing no carboxyl groups, thus surrounding the motif of interest by the oxygen atoms of both the sugar unit and the phosphate residues, respectively.

Consequently, based upon the underlying *isostructurality* we recommend to bear in mind these chemical relationships for future studies regarding structure elucidation and refinement, as well as determination of thermodynamic constants particularly by means of potentiometry and spectrophotometry.

ASSOCIATED CONTENT

Supporting Information. Additional NMR, ATR FT-IR, and EXAFS spectra, DFT-calculated structures, Speciation distribution calculations, as well as further spectroscopic and structural considerations.

AUTHOR INFORMATION

Corresponding Author

* E-mail: j.kretzschmar@hzdr.de

Present Addresses

The Federal Office for Radiation Protection, Köpenicker Allee 120-130, 10318 Berlin, Germany.

Author Contributions

The manuscript was written through contributions of all authors. All authors have given approval to the final version of the manuscript.

Notes

Any additional relevant notes should be placed here.

ACKNOWLEDGMENT

This work was partially funded by the European Union's Horizon 2020 research and innovation programme (CORI project, no. 847593) and by the German Federal Ministry for Economic Affairs and Energy (BMWi) (GRaZ II project, no. 02E11860B). We thank Aline Chlupka and Sabrina Beutner for ICP-MS measurements, Dominik Goldbach for his lab work, as well as Frank Bok for speciation calculation, and Claudia Joseph and Astrid Jäschke for valuable discussions and support.

ABBREVIATIONS

ATR FT-IR, attenuated total reflectance Fourier-transform infrared (spectroscopy); CA, citric acid; EXAFS, extended X-ray absorption fine-structure (spectroscopy); NMR, nuclear magnetic resonance (spectroscopy); U(VI), hexavalent uranium, UV-Vis, ultraviolet-visible light (absorption spectroscopy).

REFERENCES

1. Fisher, R. S., Geologic and geochemical controls on naturally occurring radioactive materials (NORM) in produced water from oil, gas, and geothermal operations. *Environ. Geosci.* **1998,** *5* (3), 139-150.

2. D. Atoufi, H.; Lampert, D. J., Impacts of Oil and Gas Production on Contaminant Levels in Sediments. *Curr. Pollut. Rep.* **2020,** *6* (2), 43-53.

3. Doyi, I.; Essumang, D. K.; Dampare, S.; Glover, E. T., Technologically Enhanced Naturally Occurring Radioactive Materials (TENORM) in the Oil and Gas Industry: A Review.

In *Reviews of Environmental Contamination and Toxicology*, de Voogt, P.; Gunther, F. A., Eds. Springer International Publishing: Cham, 2016; pp 107-119.

4. Bodansky, D., *Nuclear Energy: Principles, Practices, and Prospects*. 2nd ed.; Springer: New York, 2005.

5. Forsberg, C. W., Effect of depleted-uranium dioxide particulate fill on spent-nuclear-fuel waste packages. *Nucl. Technol.* **2000,** *131* (3), 337-353.

6. Landa, E. R.; Gray, J. R., US Geological Survey research on the environmental fate of uranium mining and milling wastes. *Environ. Geol.* **1995,** *26* (1), 19-31.

7. Duffield, J. R.; Taylor, D. M., The biochemistry of the actinides. In *Handbook on the Physics and Chemistry of the Actinides*, Freeman, A. J.; Keller, C., Eds. Elsevier B.V.: Amsterdam, 1986; Vol. 4.

8. Popplewell, D. S.; Stradling, G. N.; Ham, G. J., The Chemical Form of Plutonium in Urine. *Rad. Res.* **1975,** *62*, 513-519.

9. Duffield, J. R.; May, P. M.; Williams, D. R., Computer simulation of metal ion equilibria in biofluids. IV. plutonium speciation in human blood plasma and chelation therapy using polyaminopolycarboxylic acids. *J. Inorg. Biochem.* **1984,** *20* (3), 199-214.

10. Taylor, D. M., Acceleration of the natural rate of elimination of transuranium elements from the mammalian body. In *Handbook on the Physics and Chemistry of the Actinides*, A. J. Freeman; Keller, C., Eds. Elsevier B.V.: Amsterdam, 1991; Vol. 6.

11. Scapolan, S.; Ansoborlo, E.; Moulin, C.; Madic, C., Uranium speciation in biological medium by means of capillary electrophoresis and time-resolved laser-induced fluorescence. *J. Radioanal. Nucl. Chem.* **1997,** *226* (1), 145-148.

12. Heller, A.; Barkleit, A.; Bernhard, G., Chemical Speciation of Trivalent Actinides and Lanthanides in Biological Fluids: The Dominant in Vitro Binding Form of Curium(III) and Europium(III) in Human Urine. *Chem. Res. Toxicol.* **2011,** *24* (2), 193-203.

13. Heller, A.; Barkleit, A.; Foerstendorf, H.; Tsushima, S.; Heim, K.; Bernhard, G., Curium(iii) citrate speciation in biological systems: a europium(iii) assisted spectroscopic and quantum chemical study. *Dalton Trans.* **2012,** *41* (45), 13969-13983.

14. Lawrence, G. D.; Patel, K. S.; Nusbaum, A., Uranium toxicity and chelation therapy. *Pure Appl. Chem.* **2014,** *86* (7), 1105-1110.

15. Osman, A. A. A.; Geipel, G.; Barkleit, A.; Bernhard, G., Uranium(VI) Binding Forms in Selected Human Body Fluids: Thermodynamic Calculations versus Spectroscopic Measurements. *Chem. Res. Toxicol.* **2015,** *28* (2), 238-247.

16. Hummel, W.; Anderegg, G.; Puigdomènech, I.; Rao, L.; Tochiyama, O., *Chemical Thermodynamics of Compounds and Complexes of U, Np, Pu, Am, Tc, Se, Ni and Zr with Selected Organic Ligands*. Elsevier: Amsterdam, 2005.

17. Kretzschmar, J.; Tsushima, S.; Drobot, B.; Steudtner, R.; Schmeide, K.; Stumpf, T., Trimeric uranyl(VI)–citrate forms Na^{+}, Ca^{2+}, and La^{3+} sandwich complexes in aqueous solution. *Chem. Commun.* **2020,** *56* (86), 13133-13136.

18. Basile, M.; Unruh, D. K.; Gojdas, K.; Flores, E.; Streicher, L.; Forbes, T. Z., Chemical controls on uranyl citrate speciation and the self-assembly of nanoscale macrocycles and sandwich complexes in aqueous solutions. *Chem. Commun.* **2015,** *51* (25), 5306-5309.

19. Feldman, I.; Neuman, W. F., The Uranyl—Citrate System. I. Spectrophotometric Studies in Acid Solution1. *J. Am. Chem. Soc.* **1951,** *73* (5), 2312-2315.

20. Feldman, I.; Havill, J. R.; Neuman, W. F., Polymerization of Uranyl-Citrate, -Malate, -Tartrate and -Lactate Complexes1. *J. Am. Chem. Soc.* **1954,** *76* (18), 4726-4732.

21. Feldman, I.; North, C. A.; Hunter, H. B., Equilibrium constants for the formation of polynuclear tridentate 1:1 chelates in uranyl-malate, -citrate and -tartrate systems. *J. Am. Chem. Soc.* **1960,** *64* (9), 1224-1230.

22. Rajan, K. S.; Martell, A. E., Equilibrium Studies of Uranyl Complexes. III. Interaction of Uranyl Ion with Citric Acid. *Inorg. Chem.* **1965,** *4* (4), 462-469.

23. Kakihana, M.; Nagumo, T.; Okamoto, M.; Kakihana, H., Coordination structures for uranyl carboxylate complexes in aqueous solution studied by IR and carbon-13 NMR spectra. *J. Phys. Chem.* **1987,** *91* (24), 6128-6136.

24. Nunes, M. T.; Gil, V. M. S., New NMR evidence on the uranyl□citrate complexes. *Inorg. Chim. Acta* **1987,** *129* (2), 283-287.

25. Allen, P. G.; Shuh, D. K.; Bucher, J. J.; Edelstein, N. M.; Reich, T.; Denecke, M. A.; Nitsche, H., EXAFS Determinations of Uranium Structures: The Uranyl Ion Complexed with Tartaric, Citric, and Malic Acids. *Inorg. Chem.* **1996,** *35* (3), 784-787.

26. Pasilis, S. P.; Pemberton, J. E., Speciation and Coordination Chemistry of Uranyl(VI)−Citrate Complexes in Aqueous Solution. *Inorg. Chem.* **2003,** *42* (21), 6793-6800.

27. Günther, A.; Steudtner, R.; Schmeide, K.; Bernhard, G., Luminescence properties of uranium(VI) citrate and uranium(VI) oxalate species and their application in the determination of complex formation constants. *Radiochim. Acta* **2011,** *99* (9), 535-542.
28. Berto, S.; Crea, F.; Daniele, P. G.; De Stefano, C.; Prenesti, E.; Sammartano, S., Potentiometric and spectrophotometric characterization of the UO22+-citrate complexes in aqueous solution, at different concentrations, ionic strengths and supporting electrolytes. *Radiochim. Acta* **2012,** *100* (1), 13-28.
29. Huang, F. Y. C.; Brady, P. V.; Lindgren, E. R.; Guerra, P., Biodegradation of Uranium−Citrate Complexes: Implications for Extraction of Uranium from Soils. *Environ. Sci. Technol.* **1998,** *32* (3), 379-382.
30. Francis, A. J.; Dodge, C. J., Bioreduction of Uranium(VI) Complexed with Citric Acid by Clostridia Affects Its Structure and Solubility. *Environ. Sci. Technol.* **2008,** *42* (22), 8277-8282.
31. Crean, D. E.; Livens, F. R.; Sajih, M.; Stennett, M. C.; Grolimund, D.; Borca, C. N.; Hyatt, N. C., Remediation of soils contaminated with particulate depleted uranium by multi stage chemical extraction. *J. Hazard. Mater.* **2013,** *263*, 382-390.
32. Francis, A. J.; Dodge, C. J., Remediation of Soils and Wastes Contaminated with Uranium and Toxic Metals. *Environ. Sci. Technol.* **1998,** *32* (24), 3993-3998.
33. Kantar, C.; Honeyman, B., Citric Acid Enhanced Remediation of Soils Contaminated with Uranium by Soil Flushing and Soil Washing. *J. Environ. Eng. (ASCE)* **2006,** *132* (2), 247-255.
34. Thuery, P., Novel two-dimensional uranyl-organic assemblages in the citrate and d(-)-citramalate families. *CrystEngComm* **2008,** *10* (1), 79-85.
35. Thuery, P., Uranyl-3d block metal ion heterometallic carboxylate complexes including additional chelating nitrogen donors. *CrystEngComm* **2013,** *15* (33), 6533-6545.
36. Thuery, P., Uranyl citrate dimers as guests in a copper-bipyridine framework: a novel heterometallic inorganic-organic hybrid compound. *CrystEngComm* **2007,** *9* (5), 358-360.
37. Thuery, P., Uranyl Ion Complexation by Citric and Citramalic Acids in the Presence of Diamines. *Inorg. Chem.* **2007,** *46* (6), 2307-2315.
38. Kresge, A., Solvent isotope effect in H2O–D2O mixtures. *Pure Appl. Chem* **1964,** *8*, 243-258.

39. Lucks, C. Structure investigations of dissolved and haematite-sorbed uranium(VI) complexes of aliphatic (hydroxy) carboxylic acids: combination of various spectroscopic methods, factor analysis, and quantum chemical calculation (translated) Ph.D., Technische Universität Dresden; Helmholtz-Zentrum Dresden-Rossendorf, Institut für Ressourcenökologie, Dresden, 2012.

40. Scheinost, A. C.; Claussner, J.; Exner, J.; Feig, M.; Findeisen, S.; Hennig, C.; Kvashnina, K. O.; Naudet, D.; Prieur, D.; Rossberg, A.; Schmidt, M.; Qiu, C.; Colomp, P.; Cohen, C.; Dettona, E.; Dyadkin, V.; Stumpf, T., ROBL-II at ESRF: a synchrotron toolbox for actinide research. *J. Synchrotron Radiat.* **2021,** *28* (1), 333-349.

41. George, G. N.; Pickering, I. J. *EXAFSPAK: A Suite of Computer Programs for Analysis of X-ray Absorption Spectra*, Stanford Synchrotron Radiation Laboratory: Stanford, CA, USA, 1995.

42. Frisch, M. J., G. W. Trucks, H. B. Schlegel, G. E. Scuseria, M. A. Robb, J. R. Cheeseman, G. Scalmani, V. Barone, B. Mennucci, G. A. Petersson, H. Nakatsuji, M. Caricato, X. Li, H. P. Hratchian, A. F. Izmaylov, J. Bloino, G. Zheng, J. L. Sonnenberg, M. Hada, M. Ehara, K. Toyota, R. Fukuda, J. Hasegawa, M. Ishida, T. Nakajima, Y. Honda, O. Kitao, H. Nakai, T. Vreven, J. A. Montgomery, Jr., J. E. Peralta, F. Ogliaro, M. Bearpark, J. J. Heyd, E. Brothers, K. N. Kudin, V. N. Staroverov, R. Kobayashi, J. Normand, K. Raghavachari, A. Rendell, J. C. Burant, S. S. Iyengar, J. Tomasi, M. Cossi, N. Rega, J. M. Millam, M. Klene, J. E. Knox, J. B. Cross, V. Bakken, C. Adamo, J. Jaramillo, R. Gomperts, R. E. Stratmann, O. Yazyev, A. J. Austin, R. Cammi, C. Pomelli, J. W. Ochterski, R. L. Martin, K. Morokuma, V. G. Zakrzewski, G. A. Voth, P. Salvador, J. J. Dannenberg, S. Dapprich, A. D. Daniels, Ö. Farkas, J. B. Foresman, J. V. Ortiz, J. Cioslowski, and D. J. Fox *Gaussian 09*, Gaussian 09, Revision A.02; Gaussian Inc.: Wallingford, CT, USA, 2009.

43. Becke, A. D., Density-functional thermochemistry. III. The role of exact exchange. *J. Chem. Phys.* **1993,** *98* (7), 5648-5652.

44. Lee, C.; Yang, W.; Parr, R. G., Development of the Colle-Salvetti correlation-energy formula into a functional of the electron density. *Phys. Rev. B* **1988,** *37* (2), 785-789.

45. Barone, V.; Cossi, M., Quantum Calculation of Molecular Energies and Energy Gradients in Solution by a Conductor Solvent Model. *J. Phys. Chem. A* **1998,** *102* (11), 1995-2001.

46. Cossi, M.; Rega, N.; Scalmani, G.; Barone, V., Energies, structures, and electronic properties of molecules in solution with the C-PCM solvation model. *J. Comput. Chem.* **2003,** *24* (6), 669-681.

47. Küchle, W.; Dolg, M.; Stoll, H.; Preuss, H., Energy-adjusted pseudopotentials for the actinides. Parameter sets and test calculations for thorium and thorium monoxide. *J. Chem. Phys.* **1994,** *100* (10), 7535-7542.

48. Tsushima, S., On the "yl" bond weakening in uranyl(VI) coordination complexes. *Dalton Trans.* **2011,** *40* (25), 6732-6737.

49. Krishnan, R.; Binkley, J. S.; Seeger, R.; Pople, J. A., Self-consistent molecular orbital methods. XX. A basis set for correlated wave functions. *J. Chem. Phys.* **1980,** *72* (1), 650-654.

50. Binstead, R. A.; Zuberbühler, A. D.; Jung, B. *SPECFIT Global Analysis System*, Version 3.0.37; Spectrum Software Associates: Marlborough, MA, USA, 2005.

51. Silva, A. M. N.; Kong, X.; Hider, R. C., Determination of the pKa value of the hydroxyl group in the α-hydroxycarboxylates citrate, malate and lactate by 13C NMR: implications for metal coordination in biological systems. *BioMetals* **2009,** *22* (5), 771-778.

52. Gampp, H.; Maeder, M.; Meyer, C. J.; Zuberbühler, A. D., Calculation of equilibrium constants from multiwavelength spectroscopic data—II132, 95.: Specfit: two user-friendly programs in basic and standard fortran 77. *Talanta* **1985,** *32* (4), 257-264.

53. Clark, D. L.; Conradson, S. D.; Donohoe, R. J.; Keogh, D. W.; Morris, D. E.; Palmer, P. D.; Rogers, R. D.; Tait, C. D., Chemical Speciation of the Uranyl Ion under Highly Alkaline Conditions. Synthesis, Structures, and Oxo Ligand Exchange Dynamics. *Inorg. Chem.* **1999,** *38* (7), 1456-1466.

54. Lu, G.; Haes, A. J.; Forbes, T. Z., Detection and identification of solids, surfaces, and solutions of uranium using vibrational spectroscopy. *Coord. Chem. Rev.* **2018,** *374*, 314-344.

55. Guillaumont, R.; Fanghänel, T.; Fuger, J.; Grenthe, I.; Neck, V.; Palmer, D. A.; Rand, M. H., *Update on the Chemical Thermodynamics of Uranium, Neptunium, Plutonium, Americium and Technetium*. Elsevier: Amsterdam, 2003.

56. Winde, F.; Wade, P.; Van der Walt, I. J., Gold tailings as a source of water-borne uranium contamination of streams - The Koekemoerspruit (South Africa) as a case study. Part III of III: Fluctuations of stream chemistry and their impacts on uranium mobility. *Water SA* **2004,** *30* (2), 233-239.

57. Davies, C. W., *Ion Association*. Butterworths: London, 1962.
58. Richens, D. T.; Guille-Photin, C., Reduction of the incomplete cuboidal molybdenum(IV) aqua ion [Mo3(μ3-O)(μ-O)3(OH2)9]4+ by Eu2+. Characterisation of the trinuclear molybdenum(III) and mixed-valence molybdenum(III,III,IV) aqua ions by oxygen-17 nuclear magnetic resonance spectroscopy. *J. Chem. Soc., Dalton Trans.* **1990,** (2), 407-412.
59. Liu, W.; Liu, C.; Wu, W.; Zhang, G.; Zhang, J.; Tung, C.-H.; Wang, Y., Effects of organic ammonium cations on the isolation of {Ti4} cyclic clusters from water: an 17O NMR study. *Dalton Trans.* **2020,** *49* (18), 5957-5964.
60. Rossberg, A.; Funke, H., Determining the radial pair distribution function from X-ray absorption spectra by use of the Landweber iteration method. *J. Synchrotron Rad.* **2010,** *17* (2), 280-288.
61. Tsushima, S.; Rossberg, A.; Ikeda, A.; Müller, K.; Scheinost, A. C., Stoichiometry and Structure of Uranyl(VI) Hydroxo Dimer and Trimer Complexes in Aqueous Solution. *Inorg. Chem.* **2007,** *46* (25), 10819-10826.
62. Lucks, C.; Rossberg, A.; Tsushima, S.; Foerstendorf, H.; Scheinost, A. C.; Bernhard, G., Aqueous Uranium(VI) Complexes with Acetic and Succinic Acid: Speciation and Structure Revisited. *Inorg. Chem.* **2012,** *51* (22), 12288-12300.
63. Meinrath, G., Uranium(VI) speciation by spectroscopy. *J. Radioanal. Nucl. Chem.* **1997,** *224* (1), 119-126.
64. Quilès, F.; Burneau, A., Infrared and Raman spectra of uranyl(VI) oxo-hydroxo complexes in acid aqueous solutions: a chemometric study. *Vib. Spectrosc.* **2000,** *23* (2), 231-241.
65. Müller, K.; Brendler, V.; Foerstendorf, H., Aqueous Uranium(VI) Hydrolysis Species Characterized by Attenuated Total Reflection Fourier-Transform Infrared Spectroscopy. *Inorg. Chem.* **2008,** *47* (21), 10127-10134.
66. Ray, R. S.; Krüger, S.; Rösch, N., Uranyl monocarboxylates of aromatic acids: A density functional model study of uranyl humate complexation. *Dalton Trans.* **2009,** *0* (18), 3590-3598.
67. Ray, R. S.; Krüger, S.; Rösch, N., Ternary uranyl hydroxo acetate complexes: A computational study of structure, energetics, and stability constants. *Inorg. Chim. Acta* **2010,** *363* (1), 263-269.

68. Jung, E. C.; Cho, H.-R.; Kim, H.-K.; Cha, W., Laser-based Spectroscopic Studies of Actinide Complexes. In *The Heaviest Metals: Science and Technology of the Actinides and Beyond*, Evans, W. J.; Hanusa, T. P., Eds. John Wiley & Sons, Ltd: Hoboken, NJ, USA, 2019.
69. Lehmann, S.; Foerstendorf, H.; Zimmermann, T.; Patzschke, M.; Bok, F.; Brendler, V.; Stumpf, T.; Steudtner, R., Thermodynamic and structural aspects of the aqueous uranium(iv) system – hydrolysis vs. sulfate complexation. *Dalton Trans.* **2019,** *48* (48), 17898-17907.
70. Rajan, K. S.; Martell, A. E., Equilibrium Studies of Uranyl Complexes. III. Interaction of Uranyl Ion with Citric Acid. *Inorg. Chem.* **1965,** *4* (4), 462-469.
71. Suzuki, Y.; Nankawa, T.; Yoshida, T.; Ozaki, T.; Ohnuki, T.; Francis, A. J.; Tsushima, S.; Enokida, Y.; Yamamoto, I., Reduction behavior of uranium in the presence of citric acid. *Radiochim. Acta* **2006,** *94* (9-11), 579-583.
72. Thuéry, P.; Harrowfield, J., Uranyl Ion Complexes with Chiral Malic and Citramalic, and Prochiral Citric and Tricarballylic Acids: Influence of Coligands and Additional Metal Cations. *Eur. J. Inorg. Chem.* **2018,** *2018* (8), 1016-1027.
73. Åberg, M., The Crystal Structure of Hexaaqua-tri-mu-hydroxo-mu3-oxo-triuranyl(VI) Nitrate Tetrahydrate, [(UO2)3O(OH)3(H2O)6]NO3.4H2O. *Acta Chem. Scand. A* **1978,** *32*, 101-107.
74. Åberg, M., On the Structures of the Predominant Hydrolysis Products of Uranyl(VI) in Solution. *Acta Chem. Scand.* **1970,** *24*, 2901-2915.
75. Quilès, F.; Nguyen-Trung, C.; Carteret, C.; Humbert, B., Hydrolysis of Uranyl(VI) in Acidic and Basic Aqueous Solutions Using a Noncomplexing Organic Base: A Multivariate Spectroscopic and Statistical Study. *Inorg. Chem.* **2011,** *50* (7), 2811-2823.
76. Bell, J. T.; Biggers, R. E., The absorption spectrum of the uranyl ion in perchlorate media: Part II. The effects of hydrolysis on the resolved spectral bands. *J. Mol. Spectrosc.* **1967,** *22* (1–4), 262-271.
77. Unruh, D. K.; Gojdas, K.; Flores, E.; Libo, A.; Forbes, T. Z., Synthesis and Structural Characterization of Hydrolysis Products within the Uranyl Iminodiacetate and Malate Systems. *Inorg. Chem.* **2013,** *52* (17), 10191-10198.
78. Zhang, Y.; Clegg, J. K.; Lu, K.; Lumpkin, G. R.; Tran, T. T.; Aharonovich, I.; Scales, N.; Li, F., Uranium(VI) hybrid materials with [(UO2)3(μ3-O)(μ2-OH)3]+ as the sub–building unit via uranyl–cation interactions. *ChemistrySelect* **2016,** *1* (1), 7-12.

79. Zhang, W.; Zhao, J., A uranium–potassium-organic framework solids: Hydrothermal synthesis, structure, and property of $K[(UO_2)_3(\mu_3\text{-}OH)_3(\mu_2\text{-}OH)(C_7H_4O_4N)_2]OH$. *Inorg. Chem. Commun.* **2006,** *9* (4), 397-399.

80. Szabó, Z.; Furó, I.; Csöregh, I., Combinatorial Multinuclear NMR and X-ray Diffraction Studies of Uranium(VI)-Nucleotide Complexes. *J. Am. Chem. Soc.* **2005,** *127* (43), 15236-15247.

Table of Contents

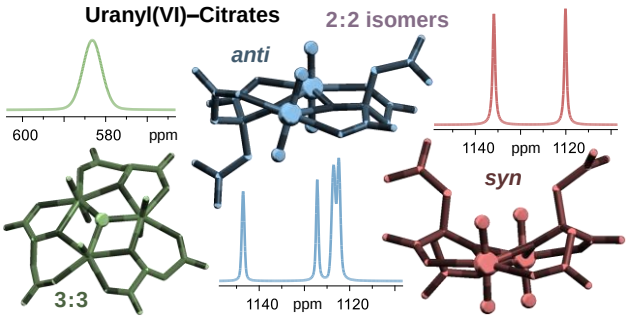

Almost 70 years of uranium–citrate research and still so much to discover: chirality, diastereomers, pH-dependent intra- and intermolecular dynamics, hydrolysis within the chelates, formation of superstructures. Especially helpful: ^{17}O NMR combined with DFT.